Fernández Domene, RM.; Blasco-Tamarit, E.; García-García, D.; Garcia-Anton, J. (2015). Effect of temperature on the passive state of Alloy 31 in a LiBr solution: Passivation and Mott-Schottky analysis. Materials and Corrosion / Werkstoffe und Korrosion. 66(11):1305-1314. doi:10.1002/maco.201508263.

EFFECT OF TEMPERATURE ON THE PASSIVE STATE OF ALLOY 31 IN A LiBr SOLUTION: PASSIVATION AND MOTT-SCHOTTKY ANALYSIS

Fernández-Domene, R.M., Blasco-Tamarit, E., García-García, D.M., García-Antón, J. *

Ingeniería Electroquímica y Corrosión (IEC). Departamento de Ingeniería Química y Nuclear. ETSI Industriales. Universitat Politècnica de València. Camino de Vera s/n, 46022 Valencia, Spain.

**Corresponding author. Tel. 34-96-387 76 32, Fax. 34-96-387 76 39,*

e-mail: jgarciaa@iqn.upv.es (J. García-Antón); raferdo1@etsii.upv.es (R.M. Fernández-Domene).

The passive behaviour of Alloy 31, a highly-alloyed austenitic stainless steel (UNS N08031), has been investigated in a LiBr heavy brine (700 g/l) at different temperatures using potentiostatic polarisation and Mott-Schottky analysis. Cation vacancies have been found to be the dominant defect in the passive films formed on Alloy 31. An increase in temperature enhanced the generation of cation vacancies at the film/solution interface and raised the steady-state passive current density. The density of defects within the passive film also increased significantly with temperature, making the film more conductive and less protective against localised attacks.

Keywords: stainless steel; passive film; semiconductor; Mott-Schottky; PDM.

1. INTRODUCTION

Energy demand for refrigeration and air-conditioning appliances has been increasing in last decades [1-3]. World energy demand as well as CO_2 emissions are expected to rise about 60% by 2030 as compared to the beginning of this century [1]. Conventional vapour compression chillers require electricity to work, which is produced from fossil fuels and therefore non-renewable sources. Additionally, vapour compression cooling systems use CFCs and HCFCs as working fluids, which contribute to global warming and ozone layer depletion. Absorption cooling systems use heat as energy source, which can be supplied by waste heat recovered from other industrial processes (e.g. in oil refineries and petrochemical facilities) or from solar energy [1, 4, 5]. Lithium bromide-water absorption cooling systems are widely used in thermal-driven air-conditioning systems and have several benefits in comparison with compression cooling systems: they require a tenth of the energy consumed by vapour compression chillers, are environmentally-friendly (the LiBr-water mixture used as a refrigerant has zero global warming potential and does not contribute to stratospheric ozone layer depletion) and noise free, among others [6, 7].

In spite of the advantages of LiBr absorption machines, bromide ions are aggressive and can cause serious corrosion problems in these refrigeration systems. Moreover, the high temperatures and concentrations reached in absorption machines accelerate the corrosive effect of bromides [8-16]. One method to solve these corrosion problems is to use high corrosion-resistant metallic materials in their construction, like highly alloyed austenitic stainless steels with large amounts of chromium, nickel and molybdenum (superaustenitic stainless steels). One of these metallic materials is Alloy 31 (UNS

N08031), with 26.75% Cr, 31.85% Ni and 6.6% Mo. Alloy 31 is characterised by its high resistance to corrosion in halide media [11, 17-19]. Nevertheless, because of the severe conditions inside absorption machines, even highly alloyed metallic materials such as Alloy 31 may undergo passivity breakdown and localised attacks [11, 18-20]. Therefore, it is very important to understand the mechanisms of formation, growth and eventual breakdown of Alloy 31 passive films in LiBr environments.

The Point Defect Model (PDM) developed by Macdonald and co-workers [21-30] is perhaps the most well-known model for the passive state nowadays. The basis for this model is that passive films are considered to be highly defective structures with the main point defects being cation vacancies ($V_M^{\chi'}$), anion vacancies (oxygen vacancies, $V_O^{\bullet\bullet}$) and/or cation interstitials ($M_i^{\chi+}$), as designated by the Kroger-Vink notation. The PDM emphasises the role of these ionic point defects in conducting the current through the film. According to the PDM, anion vacancies and cation interstitials are created and consumed at the metal/film and film/electrolyte interfaces, respectively; on the other hand, cation vacancies are created at the film/electrolyte interface but are consumed at the metal/film interface. The formation and annihilation of anion vacancies contribute to film growth (which occurs inward into the metal phase), while cation vacancies contribute to metal dissolution through the film. Passivity breakdown is closely related to the concentration of cation vacancies at the metal/film interface, and hence related to the flux of cation vacancies through the film. Consequently, the transport of vacancies within the passive film under the influence of both a concentration gradient and an electrical potential gradient is necessary for the processes of film growth and breakdown. Another important assumption of the PDM is that the

electric field strength across the film depends on the chemical and electrical properties, being independent of applied potential and film thickness.

The goal of this paper is to examine the influence of temperature on the passive behaviour and electronic properties of Alloy 31 in a heavy brine LiBr solution (700 g/l) and to find out a relationship between the electronic and corrosion properties of the passive film, through the study of current density transients and Mott-Schottky analysis (M-S).

2. EXPERIMENTAL PROCEDURE

Materials, specimen preparation and electrochemical measurements

The material tested was the highly alloyed austenitic stainless steel Alloy 31 (UNS N08031: 26.75% Cr, 31.85% Ni, 1.50% Mn, 0.10% Si, 6.60% Mo, 1.21% Cu, 31.43% Fe, 0.002% S, 0.017% P, 0.005% C, 0.193% N), provided by ThyssenKrupp VDM. The Alloy 31 electrodes were cylindrically shaped (8-mm in diameter) and covered with a polytetrafluoroethylene (PTFE) coating. The area exposed to the solution was 0.5 cm^2. All specimens were wet abraded from 500 to 4000 SiC grit, and finally rinsed with distilled water. The samples were tested in a 700 g/l (8.06 M) LiBr solution (pH = 6.80) at four different temperatures: 25, 50, 75 and 100 ºC. Before the tests, the electrolyte was purged with purified nitrogen gas for 1 hour, in order to deaerate the solution. The purging continued over the electrolyte solution until the end of the tests.

All electrochemical measurements were carried out using an Autolab PGSTAT302N potentiostat. A Ag/AgCl 3M KCl electrode served as the reference electrode and a

platinum wire served as the counter electrode. In all cases the tests were repeated at least three times in order to verify reproducibility.

Determination of the polarisability of the passive film/solution interface, α

In order to obtain the parameter α (the dependence of the potential drop across the film/ solution interface, $\phi_{f/s}$, on the applied potential, or polarisability of the passive film/solution interface), potentiodynamic polarisation curves were performed at different LiBr concentrations, from 28 to 992 g/l LiBr (0.32 – 11.42 M, respectively), and at different temperatures from 25 to 100º C (at concentrations lower than 700 g/l LiBr, the maximum temperature was 75º C, since at 100º C the solutions showed signs of boiling; thus, at 100º C only two polarisation curves were performed: 700 and 992 g/l LiBr). The potential of the working electrode was scanned from a value of -150 mV with respect to the open circuit potential towards the active direction at 0.5 mV/s. From these curves, the pitting potential E_p was determined as the potential at which the current density reached 100 $\mu A/cm^2$. The parameter α was afterwards calculated from the slope of the linear representation E_p vs. log a_{Br^-}, a_{Br^-} being the activity of bromide anions in each LiBr solution.

Potentiostatic passivation tests

Before the potentiostatic passivation tests, the surface of the samples was pre-treated cathodically at -1 $V_{Ag/AgCl}$ for 30 min to create reproducible initial conditions. Afterwards, the working electrode was polarised at different film formation potentials within the passive region of Alloy 31 (from -0.3 $V_{Ag/AgCl}$ to 0.05 $V_{Ag/AgCl}$ at 25 and 50

ºC, from -0.25 $V_{Ag/AgCl}$ to 0 $V_{Ag/AgCl}$ at 75 ºC, and from -0.2 $V_{Ag/AgCl}$ to -0.05 $V_{Ag/AgCl}$ at 100 ºC) for 1 hour to form a steady-state passive film. During passivation experiments, current density was recorded against time.

Capacitance measurements

Mott–Schottky plots were obtained by sweeping the potential from the film formation value in the negative direction with potential steps of 50 mV, at a frequency of 5 kHz with an amplitude signal of 10 mV. A high scanning rate was used to avoid electroreduction of the passive film and changes in film thickness during the measurements. At a sufficiently high scanning rate, the defect structure within the passive film is "frozen-in" to avoid defect density from being affected by the change in applied potential [27, 31, 32].

3. RESULTS AND DISCUSSION

Determination of the polarisability of the passive film/solution interface, α

The parameter α is very important in passive systems since it expresses the dependence of the potential drop across the passive film/solution interface on the applied potential [21, 22]. Therefore, α value illustrates the potential distribution at the interfaces (metal/film and film/solution). According to the PDM [33-35], the critical breakdown potential or pitting potential, E_p, can be expressed as a function of the logarithm of the aggressive anions activity, as follows:

$$E_p = \left(\frac{4.606RT}{\chi\alpha F}\right)\log\left(\frac{b}{D}\right) - \frac{2.303RT}{\alpha F}\log\left(a_{Br^-}\right) \qquad \textbf{(1)}$$

where χ is the charge of the metal ions, b is a constant and D is the diffusivity of cation vacancies in the passive film, F is Faraday's constant (96485.34 C mol^{-1}), R is the gas constant and T is absolute temperature.

Potentiodynamic polarisation curves of Alloy 31 in the different LiBr solution at 25, 50, 75 and 100º C are shown in **Figure 1**. As tests were reproducible, these curves illustrate one of the recorded measurements. It can be observed that as LiBr concentration increases, the sharp increase in current density corresponding to the pitting potential shifts towards more negative values. This result indicates worse pitting corrosion resistance of Alloy 31 in concentrated LiBr solution.

Eq. (1) predicts a linear relationship between the pitting potential and the logarithm of aggressive anions activity. The value of α can therefore be determined from the slope of this straight line. Activities for LiBr solutions, a_{LiBr}, have been calculated from the following equation:

$$a_{LiBr} = \frac{m_{LiBr}}{m^0}\gamma_{\pm} \qquad \textbf{(2)}$$

m_{LiBr} being the LiBr molality (mol LiBr/kg H_2O), m^0 is the standard LiBr molality (m^0 = 1 mol LiBr/kg H_2O) and $\gamma_{\pm}$ is the mean ionic activity coefficient of LiBr in the solution. Activity coefficients were calculated using a model developed by Meissner and Kusik for strong electrolytes in aqueous solutions at different temperatures [36, 37]. The values of m_{LiBr}, $\gamma_{\pm}$ and a_{Br^-} for the different LiBr solutions at different temperatures are shown in **Table 1**.

Figure 2 shows the E_p vs log a_{Br^-} plots at 25, 50, 75 and 100º C. The error bars included in this figure show that the E_p measurements were very reproducible. A linear decrease of E_p with log a_{Br^-} can be observed at temperatures from 25 to 75º C. This linear relationship becomes more marked with increasing temperatures. At 100º C, a correct value for the slope cannot be determined since only two potentiodynamic curves were carried out due to boiling limitations. By using eq. (1), the values of α have been calculated to be 0.80, 0.47 and 0.37 at 25, 50 and 75º C, respectively. A clear decrease of α can be observed with increasing temperatures, especially from 25 to 50º C. According to this tendency, the value of α at 100º C can be estimated to be 0.3. These values of α indicate that the potential drop at the passive film/solution interface decreases as temperature increases, which increases the potential drop at the metal/film interface. It is at the metal/film interface that the reaction of passive film formation takes place, according to the PDM [22, 24, 28].

Potentiostatic passivation tests

As an illustration, **Figure 3** shows the effects of the temperature of the solution on the current transient of Alloy 31 in the 700 g/l LiBr solution when stepping the applied potential to -0.1 V from the cathodic pretreatment at -1 V. Current density decreases exponentially with passivation time regardless of the electrolyte temperature, and eventually reaches a steady-state value (i_{SS}). It is evident from **Figure 3** that current density of Alloy 31 increases significantly with increasing temperatures from 25 to 100 ºC.

According to the PDM [28, 29, 31], the general expression for the passive current density under steady-state conditions is:

$$i_{SS} = \delta F \left[k_{\text{int}} + k_{cat} + k_{dis} \left(\frac{C_{H^+}}{C^0_{H^+}} \right)^n \right] \quad \textbf{(3)}$$

where δ is the charge of cations ejected from the passive film (3 in the case of Cr^{3+}), C_{H^+} is the proton concentration in the solution, $C^0_{H^+}$ is a standard state H^+ concentration and n is the kinetic order of the reaction of passive film dissolution with respect to $\left(C_{H^+}/C^0_{H^+}\right)$. The parameters k_{int}, k_{cat} and k_{dis} are, respectively, the rate coefficients for the reactions of formation of cation interstitials, cation vacancies and passive film dissolution. Eq. (3) suggests that the steady-state current density i_{SS} is associated with the fluxes of point defects and also with the kinetic parameters for the interfacial reactions. Hence, i_{SS} consists of three components: the first ($\delta F k_{int}$) due to the generation and transport of cation interstitials, the second ($\delta F k_{cat}$) due to the generation and transport of cation vacancies and the third $\delta F k_{dis}\left(C_{H^+}/C^0_{H^+}\right)^n$ due to the movement of oxygen vacancies. The latter term is expressed in terms of the rate of dissolution of the passive film [28-31].

According to the PDM, ln i_{SS} will vary linearly with film formation potential, E_f, provided that cation vacancies dominate ionic charge transfer through the film. For cases where cation interstitials or oxygen vacancies dominate ionic charge transfer through the film and the charge of cations ejected from the passive film (δ) is the same as the charge of cations within the passive film, $\partial \ln i_{SS}/\partial E$ will be zero. On the basis of eq. (3) and the relationship between ln i_{ss} and E_f, the PDM yields a diagnostic criterion that can be used to determine the identity of the main point defects in the passive film

[38-40]. Plots of ln i_{ss} vs E_f for Alloy 31 in the 700 g/l LiBr solution at different temperatures are shown in **Figure 4**. A linear dependence of ln i_{SS} on the film formation potential is observed in the four plots, with passive current density increasing with increasing potential. According to the diagnostic criterion mentioned above, a linear ln i_{ss} vs. E_f dependence with positive slope, as is the case of **Figure 4**, indicates that there is a preponderance of cation vacancies over cation interstitials and oxygen vacancies in the passive film formed on Alloy 31 in the 700 g/l LiBr solution, that is, the majority of the current is carried by cation vacancies.

For cation vacancy conducting films, the PDM predicts that the ln i_{SS} vs E_f relationship within the passive range has the form:

$$i_{SS} = \delta F k_{cat} = \delta F k_{cat}^{0} e^{\alpha_{cat}\alpha\delta\gamma E_f} e^{\alpha_{cat}\beta\delta\gamma pH} \quad \textbf{(4)}$$

with

$$k_{cat} = k_{cat}^{0} e^{\alpha_{cat}\alpha\delta\gamma E_f} e^{\alpha_{cat}\beta\delta\gamma pH} \quad \textbf{(5)}$$

where k_{cat}^{0} and α_{cat} are the standard rate coefficient and the transfer coefficient, respectively, for the cation ejection and cation vacancy formation reaction at the passive film/electrolyte interface ($Cr_{Cr} \rightarrow Cr^{3+} + V_{Cr}^{3'}$), α is the polarisability of the passive film/electrolyte interface (calculated above), $\gamma = F/RT$ and β is the dependence of the potential drop across the film/electrolyte interface, $\phi_{f/e}$, on pH.

According to eq. (4), a plot of ln i_{SS} vs. E_f in the passive region should be linear with a slope of $\alpha_{cat}\alpha\delta\gamma$. Using the values of α calculated in the previous section and with $\delta = 3$,

the transfer coefficient for the cation ejection and cation vacancy formation reaction at the passive film/electrolyte interface, α_{cat}, can be calculated from the values of the slope of the lines in **Figure 4**. From the intercept at 0.0 V_{SHE} of the straight line in **Figure 4** ($\ln \delta F k_{cat}^{0} + \alpha_{cat}\beta\delta\gamma pH$), the value of the standard rate coefficient for the cation ejection and cation vacancy formation reaction at the film/electrolyte interface, k_{cat}^{0}, can be calculated, with pH = 6.80 and β = -0.005 V [25, 29, 30]. The calculated values of α_{cat} and k_{cat}^{0} are presented in **Figure 5**. The change of both parameters with increasing temperature is very similar.

It can be observed from **Figure 5** that α_{cat} values are rather low at the four studied temperatures. Low values of transfer coefficients have usually been found for passive film on iron and Fe-Cr alloys [29, 41-44]. In accordance with the activated complex theory, all electrochemical processes proceed via a transition state which is less stable than both reactants and products. The transfer coefficient provides an indication of how reactant-like or product-like the transition state is in terms of its electrical behaviour (charge development). Hence, the rather low α_{cat} values indicate that the charge on the developing cation vacancy at the passive film/electrolyte interface is between 2.1-34.5%, depending on the temperature of the system; in other words, the transition state is reactant-like, that is, little different from the initial state. From a physical point of view, since the rate coefficient k for an electrochemical process depends exponentially on the electrode potential and the transfer coefficient (eq. (5)), the low values of α_{cat} indicate that a change in the formation potential, E_f, will have little effect on k.

With regard to the standard rate coefficient for the cation ejection and cation vacancy formation reaction at the film/electrolyte interface, k_{cat}^{0}, it can be observed from **Figure**

5 that its value increases abruptly with increasing electrolyte temperature, indicating that the formation of cation vacancies at the film/electrolyte interface is enhanced by rising the temperature of the system.

Capacitance results

The electrochemical capacitance of the passive system was measured as a function of the applied potential to examine the semiconducting properties and defect structure of the passive films formed on Alloy 31. Mott-Schottky analysis was performed as a function of electrolyte temperature after passive film formation at different potentials within the passive range for 1 hour. From the imaginary component of the impedance (Z'') and the CPE exponents n determined in a previous work [18], it was possible to calculate the CPE parameter, Q, and then the interfacial capacitance using the following equation [18,45]:

$$C = \frac{(Q \cdot R)^{1/n}}{R} \qquad \textbf{(6)}$$

It is important to remark that capacitance is frequency dependant [46-53]. Several causes for the frequency dispersion have been proposed: (i) a non-uniform distribution of point defects through the passive film [46, 50, 53]; (ii) the contribution of surface states to the capacitance response (adsorption of anions, e.g. chlorides, or other species) [46, 50]; (iii) the ionic part of the space charge layer, which gives a contribution only at low frequencies due to the low ionic mobility, particularly in heavily doped materials where the space charge region is very thin (passive films generally satisfy these requirements) [46, 48, 51]; (iv) dielectric relaxation phenomena which occur throughout the space charge layer and the Helmholtz layer [46, 47, 50, 52]; (v) an amorphous and

strongly disordered semiconductor nature of passive films, characterised by a high density of localised states between the valence and the conduction band and whose charging leads to a strong frequency dependent capacitance behaviour [46, 49, 51, 53]; (vi) presence of deep donor states [46, 47, 51].

In a previous study [18] it has been demonstrated that the measured capacitance for Alloy 31 in heavy brine LiBr solutions becomes almost independent of frequency at 5 kHz. Therefore, a value of 5 kHz has been used in this work to eliminate capacitance dependence on frequency.

The measured capacitance of the passive system can be written as:

$$\frac{1}{C} = \frac{1}{C_{SC}} + \frac{1}{C_H} \qquad \textbf{(7)}$$

where C_{SC} is the capacitance of the space charge layer and C_H the capacitance of the Helmholtz layer.

From eq. (7), the Mott-Schottky relations for *p*-type and *n*-type semiconductors are expressed by eqs. (8a) and (8b) respectively:

$$\frac{1}{C^2} = \frac{1}{C_H^2} - \frac{2}{\varepsilon\varepsilon_0 e N_A}\left(E - E_{FB} - \frac{kT}{e}\right) \qquad \textbf{\textit{p}-type} \qquad \textbf{(8a)}$$

$$\frac{1}{C^2} = \frac{1}{C_H^2} + \frac{2}{\varepsilon\varepsilon_0 e N_D}\left(E - E_{FB} - \frac{kT}{e}\right) \qquad \textbf{\textit{n}-type} \qquad \textbf{(8b)}$$

where ε is the dielectric constant of the passive film (a value of 15.6 has been assumed for the chromium and iron oxides formed on austenitic stainless steels [46]), ε_0 is the vacuum permittivity ($8.85 \cdot 10^{-14}$ F/cm), e is the electron charge ($1.602 \cdot 10^{-19}$ C), N_A and N_D are respectively the acceptor and donor densities, E_{FB} is the flat-band potential, k is the Boltzmann constant ($1.38 \cdot 10^{-23}$ J/K) and T is the absolute temperature.

Figure 6 shows the Mott-Schottky plots of the passive films formed on Alloy 31 at different formation potentials and temperatures. In general, two different regions with different capacitance response can be observed, below and above the flat-band potential, E_{FB} (Regions I and II, respectively). In both regions, a Mott-Schottky type behaviour can be observed, that is, a linear relationship between C^{-2} and E. In the more cathodic region (Region I, $E<E_{FB}$), the slope of the linear zone is negative (only discernible at 25 and 50 ºC) and the capacitance describes the behaviour of a *p*-type semiconductor, according to eq. (8a). On the other hand, in Region II ($E > E_{FB}$), the slope of the linear zone is positive, indicating the properties of a *n*-type semiconductor. It is widely accepted that the semiconducting behaviour of Fe-Cr and Fe-Cr-Ni alloys reflects a duplex structure of passive films [19, 49, 52, 54-57]. This structure has been found to be rather complex, especially in highly alloyed stainless steels [19, 49, 56, 58-64]. The formation of a ternary inner Fe-Cr-Ni oxide layer with spinel structure has been proposed in the literature for passive films formed on highly alloyed stainless steels and nickel-base alloys [19, 49, 64, 65]. The inner layer of the passive film displays both *p*-type and *n*-type semiconductivity. In the region close to the metal surface, the spinel oxide is enriched in Cr and behaves as a *p*-type semiconductor [65]. As the Cr content in the passive film decreases and Fe content increases near the outer hydroxide layer of

the film, the spinel structure changes gradually from $NiCr_2O_4$ to $NiFe_2O_4$, which has an inverse structure and behaves as an *n*-type semiconductor [65-69]. The outer layer of the passive film consists of a mixture of Cr and Fe hydroxides and oxy-hydroxides with *n*-type semiconductivity too.

Thus, the capacitance response observed in Region I (**Figure 6**) is controlled by the electric structure of the mixed Fe-Cr-Ni spinel oxide in the region of the passive film close to the metal surface, whose dominant acceptor species are cation (chromium) vacancies, $V_{Cr}^{3'}$. The behaviour observed in Region II is controlled by the electric structure of the Fe-Cr-Ni spinel oxide with a higher amount of Fe present in the inner region of the passive film near the outer hydroxide layer, whose predominant donor species are oxygen vacancies, $V_O^{\bullet\bullet}$, and/or cation interstitials, $M_i^{\chi+}$. Fe and Cr hydroxides present in the outer region of the film may also influence the *n*-type semiconducting behaviour observed in Region II.

As mentioned above, the Mott-Schottky type behaviour in Region I is only discernible at low temperatures (**Figures 6a** and **6b**), especially at 25 ºC. At these two temperatures the slopes of the straight lines in Region I increase with formation potential. It has been reported in the literature [65, 70-74] that the concentration of Cr(III) in the passive films formed on stainless steels, Ni-Cr alloys and pure Cr increases with increasing formation potential within the passive region. The increase of Cr(III) within the passive film implies a decrease in the number of cation vacancies, $V_{Cr}^{3'}$, and consequently higher negative slopes in the *p*-type semiconductivity zone below the E_{FB} (Region I) according to eq. (8a). The absence of a linear zone with negative slope in Region I at high temperatures (**Figures 6c** and **6d**), can be explained in terms of a higher concentration

of $V_{Cr}^{3'}$ in the Cr-enriched layer of the passive film close to the metal surface. As it has been observed above (**Figure 5**), the rate of cation vacancies formation is significantly enhanced at 75 and 100 ºC, which results in an increase of $V_{Cr}^{3'}$ density. As a consequence, at high temperatures the innermost layer of the passive film is highly defective and no longer behaves as a semiconductor, but as a metal-like conductor. In Region II of **Figure 6**, the main effect of the solution temperature is a substantial increase in capacitance values (a decrease in C^{-2}), which indicates an increase in the conductivity of the Fe-enriched spinel oxide layer or a decrease in the thickness of this layer with temperature, as it will be explained below.

Acceptor and donor densities (N_A and N_D) can be determined for *p*-type and *n*-type semiconductors from the slopes of the linear zones in Regions I and II (**Figure 6**) using equations (8a) and (8b), respectively. **Figure 7** shows the values of N_A and N_D at different formation potentials and temperatures.

It can be seen from **Figure 7** that the density of defects is of the order of 10^{20}-10^{21} cm^{-3}, similar to the results obtained by other authors for stainless steels [18, 54, 60, 75, 76]. The density of cation vacancies, N_A, is always higher than the density of oxygen vacancies or cation interstitials, N_D, regardless of the solution temperature. This fact can be related to the presence of bromide anions in the solution. According to the PDM [22, 33], aggressive anions such as bromides adsorb into the surface oxygen vacancies:

$$V_O^{\bullet\bullet} + Br^- \rightarrow Br_O^{\bullet} \qquad \textbf{(9)}$$

where $Br_O^{\bullet}$ represents a bromide anion adsorbed into an oxygen vacancy in the film/electrolyte interface. The system responds to the loss of oxygen vacancies by generating cation vacancy/oxygen vacancy pairs via a Schottky-pair type of reaction:

$$\text{Null} \rightarrow V_M^{\chi'} + \left(\frac{\chi}{2}\right) V_O^{\bullet\bullet} \qquad \textbf{(10)}$$

where $V_M^{\chi'}$ represents a generic cation vacancy. The oxygen vacancies continue reacting with additional Br^- at the film/electrolyte interface to generate additional cation vacancies. Hence, the generation of cation vacancies through eqs. (9) and (10) is autocatalytic.

The higher density of cation vacancies over oxygen vacancies and metal interstitials is consistent with the result obtained from the diagnostic criterion of the PDM concerning the relationship between ln i_{SS} and E_f, explained above (eq. (4)). This criterion has been used to identify the predominant crystallographic defect type within the passive film, which has been found to be cation vacancy. However, although cation vacancies are the main defects within the passive film and determine the *p*-type semiconductivity of the innermost layer, Mott-Schottky analysis has also revealed an *n*-type semiconducting behaviour, with oxygen vacancies and/or cation interstitials acting as donor species. Therefore, the diagnostic criteria provided by the PDM should be used along with the Mott-Schottky analysis to avoid possible ambiguities [18].

Regarding the influence of temperature on the density of defects within the passive film, it can be observed from **Figure 7** that N_A and N_D increase with increasing temperatures,

indicating a more disordered structure and hence worse protective properties of passive films formed at high temperatures. The increase of N_A and N_D with temperature can be explained considering the influence of temperature on the rate coefficients for vacancy generation reactions. It has been demonstrated above that the rate coefficient for the cation vacancy formation reaction, k_{cat}^{0}, increases markedly with increasing solution temperatures (**Figure 5**). Moreover, temperature will also enhance the generation of cation vacancies via eqs. (9) and (10) [31], which accounts for the more pronounced increase of N_A with temperature and the higher degree of degeneration of the *p*-type layer of the passive film. At 75 and 100 ºC, N_A is extremely high and cannot be determined unequivocally by Mott-Schottky analysis, since at these temperatures the structure of the region of the film close to the metal surface is very degenerate and M-S approximation becomes invalid.

The $1/C^2$ vs. E plots shown in **Figure 6** exhibit a minimum in the flat-band potential region. Therefore, the measured capacitance should not be derived from a single space charge region, but from two regions [18, 48, 77]. In a metal/film/electrolyte system, space charge regions can be formed in the film either at the film/electrolyte interface or at the metal/film interface [78]. Therefore, according to the results of M-S analysis, two space charge regions appear at the metal/inner layer and outer layer/electrolyte interfaces. The capacitance of these space charge regions, C_{SC}, can be obtained from the measured capacitance values using eq. (7).

It is usually assumed that the Helmholtz layer capacitance is so large compared with the space charge layer capacitance that the total capacitance measured can be treated as the space charge layer capacitance and the potential drop caused by the applied potential

occurs entirely within the space charge region. However, charging of the Helmholtz layer capacitance cannot always be neglected. In fact, several studies [79, 80] have demonstrated that a significant part of the potential difference at the semiconductor/electrolyte interface extends to the Helmholtz layer in the solution. Therefore, C_H should not be neglected, particularly in highly doped semiconductors, such as passive films [18, 52, 80]. It can be assumed that at $E = E_{FB}$, C_H is equal to the total measured capacitance, since no depletion layer exists at this potential and the contribution of the space charge or the passive film to the total capacitance values is negligible [47, 81]. From **Figure 6** C_H values were estimated to be 15-24 μF cm^{-2} at 25 ºC, 32-42 μF cm^{-2} at 50 ºC, 47-54 μF cm^{-2} at 75 ºC and 60-76 μF cm^{-2} at 100 ºC.

The thickness of the space charge layers formed within the passive film can be calculated from the C_{SC} values determined at the formation potential (thickness of the *n*-type space charge layer) and at the most negative potential (thickness of the *p*-type space charge layer). Thicknesses have been calculated with the expression for a parallel plane condenser [48, 82]:

$$C_{SC} = \frac{\varepsilon \cdot \varepsilon_0}{W} \qquad \textbf{(11)}$$

where W is the space charge layer thickness. **Table 2** gives the thickness values of the space charge layers formed within the passive film (*p*-type layer and *n*-type layer, W_p and W_n, respectively) for Alloy 31 at different film formation potentials and temperatures. It can be observed that the thickness of the space charge layers increases with increasing formation potentials, regardless of the temperature of the system. This increase is more pronounced in the case of the *n*-type layer (W_n), which is coherent with

the higher degree of defectiveness of the *p*-type layer. In fact, at 75 and 100 ºC the thickness of the space charge layer developed in the region of the film near the metal (W_p) cannot be calculated from the space charge layer capacitances, since at these high temperatures this layer no longer behaves as a semiconductor (**Figures 6c** and **6d**). As a consequence, at 75 and 100 ºC, only the thickness of the *n*-type layer has been calculated from capacitance measurements. It can also be observed from **Table 2** that W_p and W_n decrease significantly with increasing temperatures, which is closely related to the higher density of defects found in the passive films formed at higher temperatures (**Figure 7**). These films are less compact, more conductive and have worse protective properties than those formed at lower temperatures.

The magnitude of the total thickness of the space charge layers developed within the passive films (**Table 2**) is in good agreement with the thickness of passive films formed on stainless steels, which is in the range of 1-3 nm [59]. **Figure 8** shows the variation of the total thickness of both space charge regions ($W_{SC} = W_p + W_n$) with film formation potential at different temperatures. There is a linear relationship between W_{SC} and E_f, indicating that the electric field across the space charge regions is constant and independent of the applied formation potential. A decrease in W_{SC} with increasing temperatures can also be observed. Several authors working with passive systems [31, 83] have observed an increase in the passive film thickness with increasing temperatures, in spite of the higher conductivity due to a rise in the density of charge carriers. Hence, the decrease of the total thickness of the space charge layers (W_{SC}) with increasing temperatures clearly indicates that this thickness cannot be regarded as the thickness of the whole passive film, but as an "effective thickness" directly related to the degree of degeneration and to the protective properties of the passive film.

4. CONCLUSIONS

The polarisability of the passive film/solution interface, α, decreases from 0.8 (25º C) to 0.3 (100º C). These values indicate that the fraction of the applied potential which drops in the Helmholtz layer decreases with increasing temperatures, increasing therefore the potential drop at the metal/film interface.

The logarithm of the steady-state current density, ln i_{SS}, increases linearly with applied potential at the four studied temperatures. According to the PDM, this result indicates that cation vacancies are the dominant defect in the passive films formed anodically on Alloy 31 in a 700 g/l LiBr solution.

The standard rate coefficient for the reaction of cation vacancies formation at the film/solution interface, k^0_{cat}, increases abruptly with increasing temperatures. Thus, as temperature rises, the number of cation vacancies generated at the film/solution interface will increase. This increase in k^0_{cat} results in an increase of the steady-state passive current density with temperature.

The density of defects within the passive film increases significantly with temperature, especially the density of cation vacancies in the region of the passive film close to the metal surface. At 75 and 100º C, the innermost region becomes highly defective and its electronic behaviour resembles that of a metal-like conductor.

The thickness of the space charge layers developed at the interfaces decreases with increasing temperatures. This is closely related to the higher density of defects found in the passive films formed at high temperatures, which are more conductive and have worse protective properties than those formed at lower temperatures. This result indicates that the total thickness of the space charge layers (W_{SC}) cannot be regarded as the thickness of the whole passive film, but as an "effective thickness" directly related to the degree of degeneration and to the protective properties of the passive film.

ACKNOWLEDGEMENTS

We wish express our gratitude to the Ministerio de Ciencia e Innovación (Project CTQ2009-07518), for the economical support of this research, to Thyssen Krupp for supplying the materials, and to Dr. M. Asunción Jaime for her translation assistance.

REFERENCES

[1] P. Bermejo, F. J. Pino, F. Rosa, *Sol. Energy* **2010**, *84*, 1503.

[2] U. Desideri, S. Proietti, P. Sdringola, *Appl. Energ.* **2009**, *86*, 1376.

[3] Z. S. Lu, R. Z. Wang, Z. Z. Xia, X. R. Lu, C. B. Yang, Y. C. Ma, G. B. Ma, *Renew. Energ.* **2013**, *50*, 299.

[4] Y. Fan, L. Luo, B. Souyri, *Renew. Sust. Energ. Rev.* **2007**, *11*, 1758.

[5] L. Garousi Farshi, S. M. S. Mahmoudi, M. A. Rosen, M. Yari, M. Amidpour, *Energ. Convers. Manage.* **2013**, *65*, 13.

[6] S. Popli, P. Rodgers, V. Eveloy, *Appl. Therm. Eng.* **2013**, *50*, 918.

[7] S. Jiangzhou, R. Z. Wang, *Appl. Therm. Eng.* **2001**, *21*, 1161.

[8] J. L. Guiñón, J. García-Antón, V. Pérez-Herranz, G. Lacoste, *Corrosion* **1994**, *50*, 240.

[9] A. Igual-Muñoz, J. García-Antón, S. López Nuévalos, J. L. Guiñón, V. Pérez-Herranz, *Corros. Sci.* **2004**, *46*, 2955.

[10] E. Blasco-Tamarit, A. Igual-Muñoz, J. García-Antón, D. M. García-García, *Corros. Sci.* **2006**, *48*, 863.

[11] E. Blasco-Tamarit, A. Igual-Muñoz, J. García-Antón, D. García-García, *Corros. Sci.* **2008**, *50*, 1848.

[12] V. Guiñón-Pina, A. Igual-Muñoz, J. García-Antón, *Corros. Sci.* **2009**, *51*, 2406.

[13] R. Leiva-García, M. J. Muñoz-Portero, J. García-Antón, *Corros. Sci.* **2010**, *52*, 950.

[14] R. Sánchez-Tovar, M. T. Montañés, J. García-Antón, *Corros. Sci.* **2010**, *52*, 722.

[15] R. M. Fernández-Domene, E. Blasco-Tamarit, D. M. García-García, J. García-Antón, *Corros. Sci.* **2012**, *63*, 304.

[16] R. M. Fernández-Domene, E. Blasco-Tamarit, D. M. García-García, J. García-Antón, *Electrochim. Acta* **2011**, *58*, 264.

[17] R. M. Fernández-Domene, E. Blasco-Tamarit, D. M. García-García, J. García-Antón, *Corros. Sci.* **2012**, *55*, 40.

[18] R. M. Fernández-Domene, E. Blasco-Tamarit, D. M. García-García, J. García-Antón, *Electrochim. Acta* **2013**, *95*, 1.

[19] R. M. Fernández-Domene, E. Blasco-Tamarit, D. M. García-García, J. García-Antón, *Thin Solid Films* **2014**, *558*, 252.

[20] E. Blasco-Tamarit, D. M. García-García, J. García-Antón, *Corros. Sci.* **2011**, *53*, 784.

[21] C. Y. Chao, L. F. Lin, D. D. Macdonald, *J. Electrochem. Soc.* **1981**, *128*, 1187.

[22] D. D. Macdonald, *J. Electrochem. Soc.* **1992**, *139*, 3434.

[23] E. Sikora, J. Sikora, D. D. Macdonald, *Electrochim. Acta* **1996**, *41*, 783.

[24] D. D. Macdonald, *Pure Appl. Chem.* **1999**, *71*, 951.

[25] D. D. Macdonald, A. Sun, N. Priyantha, P. Jayaweera, *J. Electroanal. Chem.* **2004**, *572*, 421.

[26] I. Nicic, D. D. Macdonald, *J. Nucl. Mater.* **2008**, *379*, 54.

[27] J. Sikora, E. Sikora, D. D. Macdonald, *Electrochim. Acta* **2000**, *45*, 1875.

[28] D. D. Macdonald, *Electrochim. Acta* **2011**, *56*, 1761.

[29] D. D. Macdonald, A. Sun, *Electrochim. Acta* **2006**, *51*, 1767.

[30] D. D. Macdonald, *J. Nucl. Mater.* **2008**, *379*, 24.

[31] K. Park, S. Ahn, H. Kwon, *Electrochim. Acta* **2011**, *56*, 1662.

[32] Z. Jiang, X. Dai, H. Middleton, *Mater. Chem. Phys.* **2011**, *126*, 859.

[33] L. F. Lin, C. Y. Chao, D. D. Macdonald, *J. Electrochem. Soc.* **1981**, *128*, 1194.

[34] T. Haruna, D. D. Macdonald, *J. Electrochem. Soc.* **1997**, *144*, 1574.

[35] Y. Zhang, D. D. Macdonald, M. Urquidi-Macdonald, G. R. Engelhardt, R. B. Dooley, *Corros. Sci.* **2006**, *48*, 3812.

[36] H. P. Meissner, J.W. Tester, *Ind. Eng. Chem. Process Des. Develop.* **1972**, *11*, 128.

[37] H. P. Meissner, C. L. Kusik, J. W. Tester, *AIChE J.* **1972**, *18*, 661.

[38] D. D. Macdonald, M. Urquidi-Macdonald, *J. Electrochem. Soc.* **1990**, *137*, 2395.

[39] D. D. Macdonald, S. R. Biaggio, H. Song, *J. Electrochem. Soc.* **1992**, *139*, 170.

[40] E. Sikora, D. D. Macdonald, *Solid State Ionics* **1997**, *94*, 141.

[41] X. Zhang, J. C. Wren, I. Betova, M. Bojinov, *Electrochim. Acta* **2011**, *56*, 5910.

[42] M. Metikos-Hukovic, R. Babic, Z. Grubac, Z. Petrovic, N. Lajçi, *Corros. Sci.* **2011**, *53*, 2176.

[43] S. J. Ahn, H. S. Kwon, D. D. Macdonald, *J. Electrochem. Soc.* **2005**, *152*, B482.

[44] Y. Zhang, M. Urquidi-Macdonald, G. R. Engelhardt, D. D. Macdonald, *Electrochim. Acta* **2012**, *69*, 1.

[45] C. Valero Vidal, A. Igual-Muñoz, *Electrochim. Acta* **2010**, *55*, 8445.

[46] A. D. Paola, *Electrochim. Acta* **1989**, *34*, 203.

[47] W. P. Gomes, D. Vanmaekelbergh, *Electrochim. Acta* **1996**, *41*, 967.

[48] M. Da Cunha Belo, N. E. Hakiki, M. G. S. Ferreira, *Electrochim. Acta* **1999**, *44*, 2473.

[49] T. L. S. Wijesinghe, D. J. Blackwood, *Corros. Sci.* **2008**, *50*, 23.

[50] J. Amri, T. Souier, B. Malki, B. Baroux, *Corros. Sci.* **2008**, *50*, 431.

[51] L. Hamadou, A. Kadri, N. Benbrahim, *Appl. Surf. Sci.* **2005**, *252*, 1510.

[52] N. E. Hakiki, S. Boudin, B. Rondot, M. Da Cunha Belo, *Corros. Sci.* **1995**, *37*, 1809.

[53] D. G. Li, J. D. Wang, D. R. Chen, *Electrochim. Acta* **2012**, *60*, 134.

[54] N. E. Hakiki, M. Da Cunha Belo, A. M. P. Simoes, M. G. S. Ferreira, *J. Electrochem. Soc.* **1998**, *145*, 3821.

[55] I. Olefjord, B. Brox, U. Jelvestam, *J. Electrochem. Soc.* **1985**, *132*, 2854.

[56] G. Lothongkum, S. Chaikittisilp, A. W. Lothongkum, *Appl. Surf. Sci.* **2003**, *218*, 203.

[57] L. Freire, M. J. Carmezim, M. G. S. Ferreira, M. F. Montemor, *Electrochim. Acta* **2010**, *55*, 6174.

[58] T. L. S. Wijesinghe, D. J. Blackwood, *Appl. Surf. Sci.* **2006**, *253*, 1006.

[59] C.-O. A. Olsson, D. Landolt, *Electrochim. Acta* **2003**, *48*, 1093.

[60] M. J. Carmezim, A. M. P. Simoes, M. F. Montemor, M. Da Cunha Belo, *Corros. Sci.* **2005**, *47*, 581.

[61] Z. Feng, X. Cheng, C. Dong, L. Xu, X. Li, *Corros. Sci.* **2010**, *52*, 3646.

[62] S. Ningshen, U. Kamachi Mudali, V. K. Mittal, H. S. Khatak, *Corros. Sci.* **2007**, *49*, 481.

[63] M. Da Cunha Belo, B. Rondot, C. Compere, M. F. Montemor, A. M. P. Simoes, M. G. S. Ferreira, *Corros. Sci.* **1998**, *40*, 481.

[64] T. L. S. L. Wijesinghe, D. J. Blackwood, *J. Electrochem. Soc.* **2007**, *154*, C16.

[65] T. Dan, T. Shoji, Z. Lu, K. Sakaguchi, J. Wang, E. H. Han, W. Ke, *Corros. Sci.* **2010**, *52*, 1228.

[66] B. Beverskog, I. Puigdomenech, *Corrosion* **1999**, *55*, 1077.

[67] M. Da Cunha Belo, M. Walls, N. E. Hakiki, J. Corset, E. Picquenard, G. Sagon, D. Noël, *Corros. Sci.* **1998**, *40*, 447.

[68] Y. H. Hou, Y.L. Zhao, Z.W. Liu, H.Y. Yu, X.C. Zhong, W.Q. Qiu, D.C. Zeng, L.S. Wen, *J. Phys. D: Appl. Phys.* **2010**, *43*, 445003 (7pp).

[69] S. H. Lee, S. J. Yoon, G. J. Lee, H. S. Kim, C. H. Yo, K. Ahn, D. H. Lee, K. H. Kim, *Mater. Chem. Phys.* **1999**, *61*, 147.

[70] L. Wegrelius, F. Falkenberg, I. Olefjord, *J. Electrochem. Soc.* **1999**, *146*, 1397.

[71] A. C. Lloyd, J. J. Noël, S. McIntyre, D. W. Shoesmith, *Electrochim. Acta* **2004**, *49*, 3015.

[72] M. Uemura, T. Yamamoto, K. Fushimi, Y. Aoki, K. Shimizu, H. Habazaki. *Corros. Sci.* **2009**, *51*, 1554.

[73] N. Padhy, R. Paul, U. Kamachi Mudali, B. Raj, *Appl. Surf. Sci.* **2011**, *257*, 5088.

[74] C. Sunseri, S. Piazza, F. Di Quarto, *J. Electrochem. Soc.* **1990**, *137*, 2411.

[75] I. Toor, J. Y. Kwon, H. S. Kwon, *J. Electrochem. Soc.* **2008**, *155*, C495.

[76] L. Pons, M. L. Délia, R. Basséguy, A. Bergel, *Electrochim. Acta* **2011**, *56*, 2682.

[77] H. Tsuchiya, S. Fujimoto, O. Chihara, T. Shibata, *Electrochim. Acta* **2002**, *47*, 4357.

[78] A. Goossens, M. Vazquez, D. D. Macdonald, *Electrochim. Acta* **1996**, *41*, 35.

[79] J. O. Bockris, *J. Appl. Phys.* **1981**, *52*, 808.

[80] K. Uosaki, H. Kita, *J. Electrochem. Soc.* **1983**, *130*, 895.

[81] N. E. Hakiki, M. Da Cunha Belo, *J. Electrochem. Soc.* **1996**, *143*, 3088.

[82] J. Pan, C. Leygraf, R. F. A. Jargelius-Pettersson, J. Linden, *Oxid. Met.* **1998**, *50*, 431.

[83] A. M. P. Simoes, M. G. S. Ferreira, G. Lorang, M. Da Cunha Belo, *Electrochim. Acta* **1991**, *36*, 315.

Tables captions

Table 1. Values of molality, m_{LiBr}, mean ionic activity coefficient, $\gamma_{\pm}$, and activity, a_{LiBr}, of LiBr solutions at different temperatures.

Table 2. Thicknesses of the *p*-type (W_p) and *n*-type (W_n) space charge layers developed in the passive films formed on Alloy 31 in the 700 g/l LiBr solution, at different temperatures and at different film formation potentials within the passive region.

Figures captions

Fig. 1. Potentiodynamic polarisation curves of Alloy 31 in the different LiBr solutions at (a) 25º C, (b) 50º C, (c) 75º C and (d) 100º C.

Fig. 2. Plots of pitting potential, E_p, versus logarithm of LiBr activity, ln a_{LiBr}, for Alloy 31 at different temperatures.

Fig. 3. Effect of solution temperature on the current transient of Alloy 31 in the 700 g/l LiBr solution when stepping the applied potential from a cathodic value of -1 $V_{Ag/AgCl}$ to a passive value of -0.1 $V_{Ag/AgCl}$.

Fig. 4. Plots of logarithm of the steady-state passive current density, ln i_{ss}, versus film formation potential, E_f, for Alloy 31 in the 700 g/l LiBr solution at different temperatures.

Fig. 5. Calculated values of the transfer coefficient α_{cat} and the standard rate coefficient k^0_{cat} for the cation vacancy formation reaction at the passive film/electrolyte interface, for Alloy 31 in the 700 g/l LiBr solution at different temperatures.

Fig. 6. Mott-Schottky plots of Alloy 31 in the 700 g/l LiBr solution at different film formation potentials and at (a) 25 ºC, (b) 50º C, (c) 75º C and (d) 100º C.

Fig. 7. (a) Acceptor and (b) donor densities for Alloy 31 in the 700 g/l LiBr solution at different temperatures and at different film formation potentials within the passive region.

Fig. 8. Estimated values of the total thickness of the space charge regions developed in the passive film of Alloy 31 (W_{SC}) as a function of the film formation potential, in the 700 g/l LiBr solution at different temperatures.

Figure 1

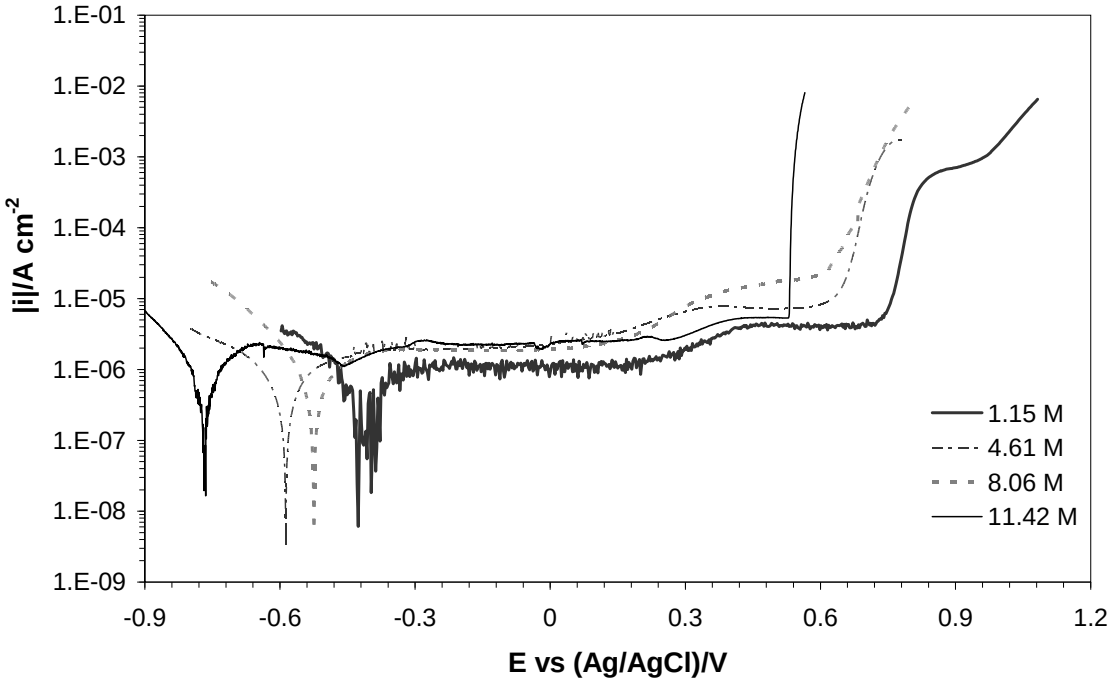
1.E-01
1.E-02
1.E-03
1.E-04
1.E-05
1.E-06
1.E-07
1.E-08
1.E-09
|i|/A cm-2
-0.9
-0.6
-0.3
0
0.3
0.6
0.9
1.2
E vs (Ag/AgCl)/V
1.15 M
4.61 M
8.06 M
11.42 M

(a)

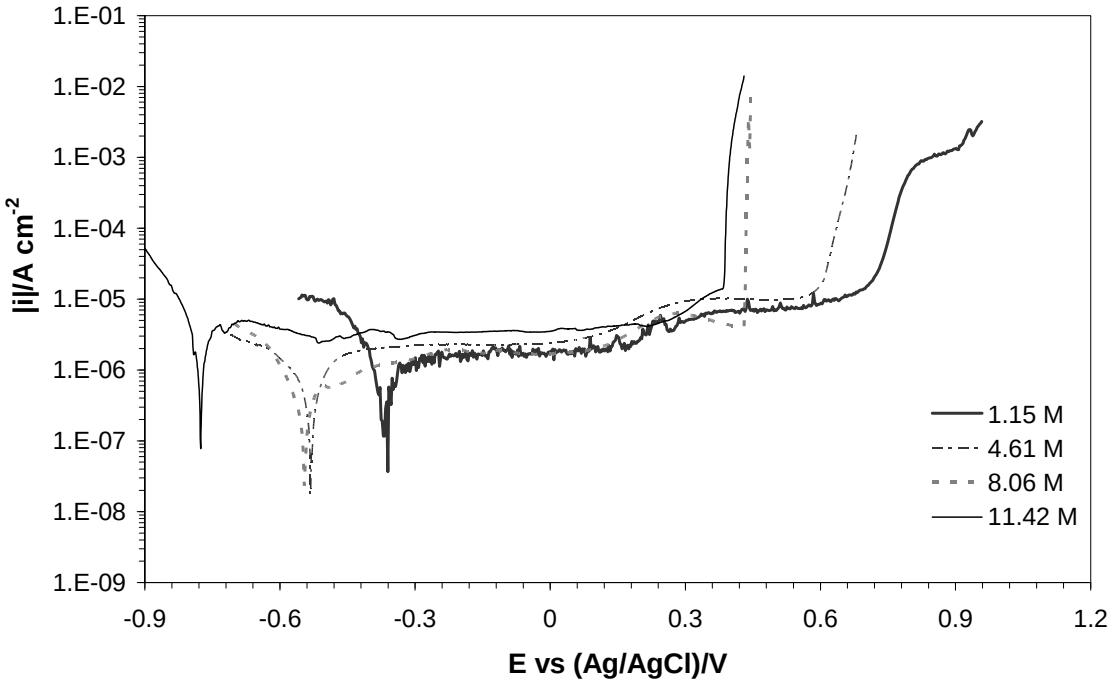
1.E-01
1.E-02
1.E-03
1.E-04
1.E-05
1.E-06
1.E-07
1.E-08
1.E-09
|i|/A cm-2
-0.9
-0.6
-0.3
0
0.3
0.6
0.9
1.2
E vs (Ag/AgCl)/V
1.15 M
4.61 M
8.06 M
11.42 M

(b)

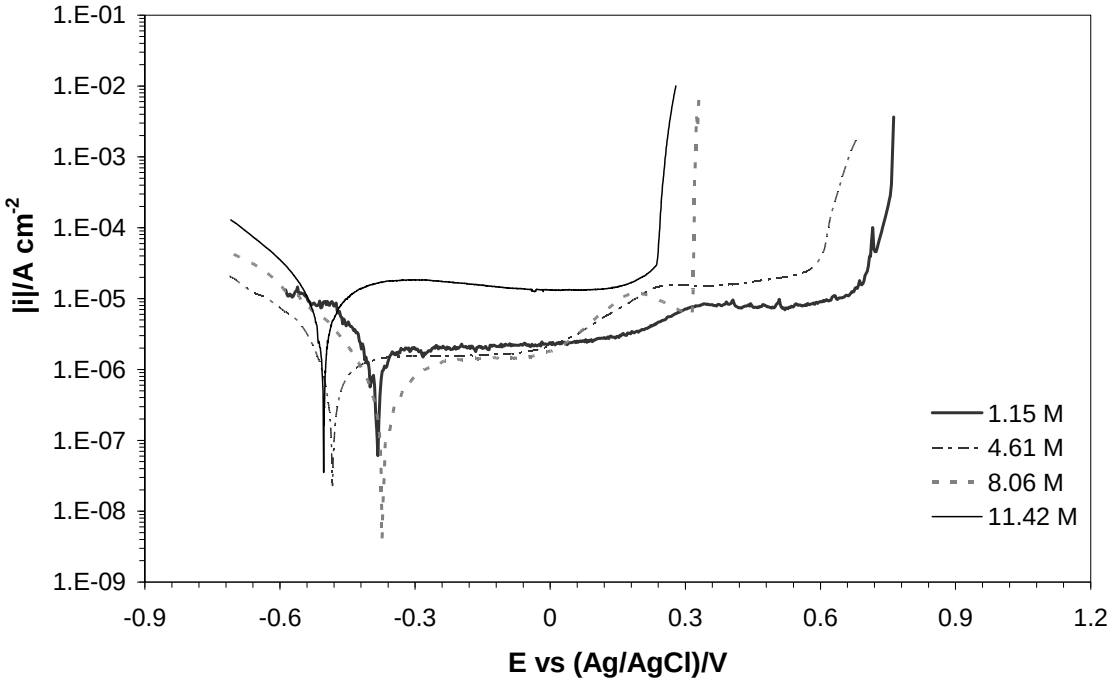
1.E-01
1.E-02
1.E-03
1.E-04
1.E-05
1.E-06
1.E-07
1.E-08
1.E-09
|i|/A cm-2
-0.9
-0.6
-0.3
0
0.3
0.6
0.9
1.2
E vs (Ag/AgCl)/V
1.15 M
4.61 M
8.06 M
11.42 M

(c)

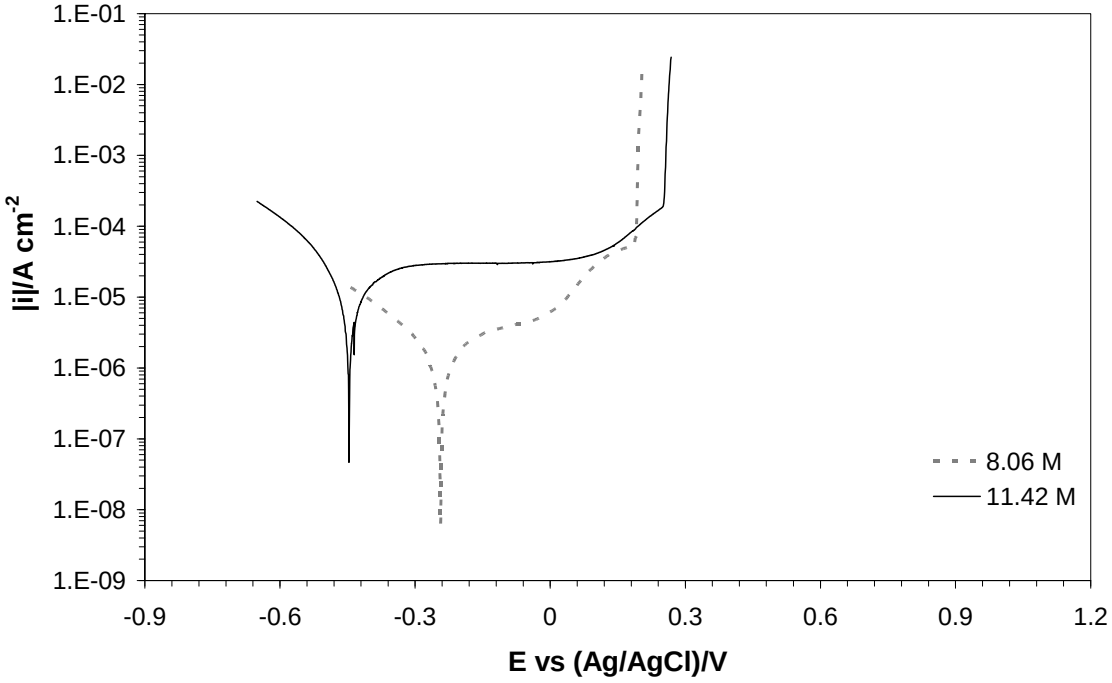
1.E-01
1.E-02
1.E-03
1.E-04
1.E-05
1.E-06
1.E-07
1.E-08
1.E-09
|i|/A cm-2
-0.9
-0.6
-0.3
0
0.3
0.6
0.9
1.2
E vs (Ag/AgCl)/V
8.06 M
11.42 M

(d)

Figure 2

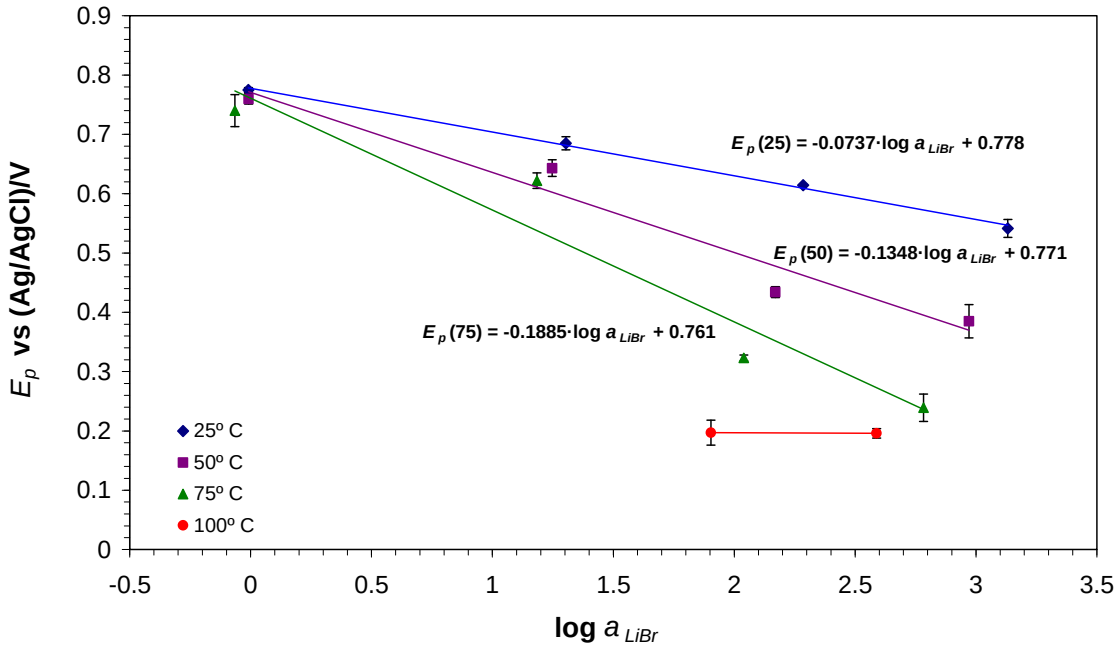

Figure 3

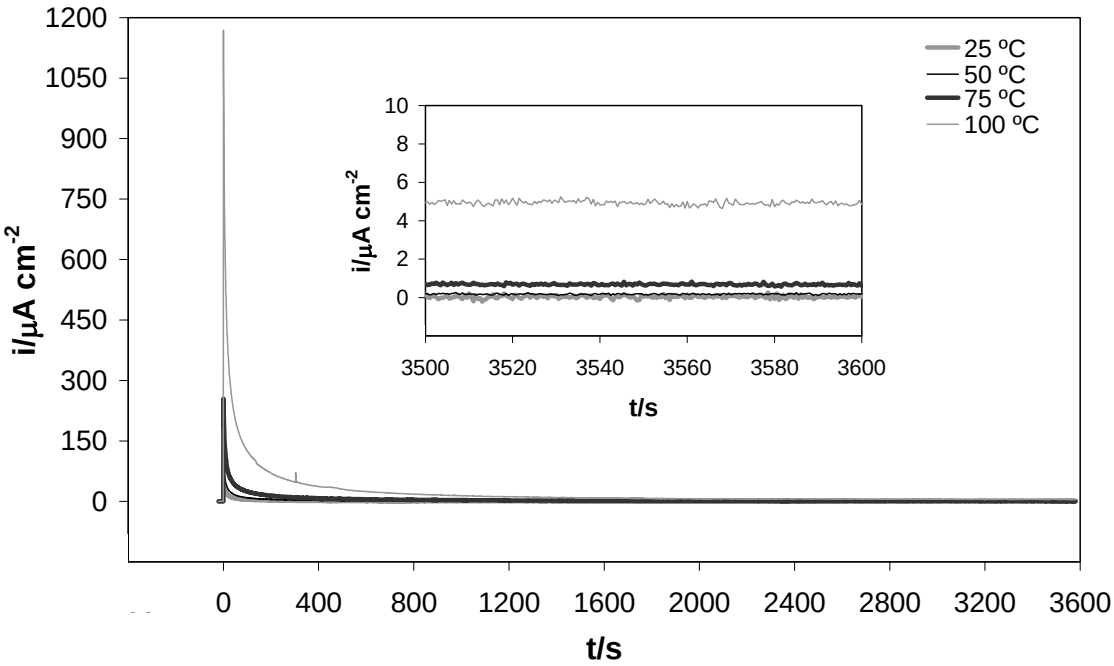

Figure 4

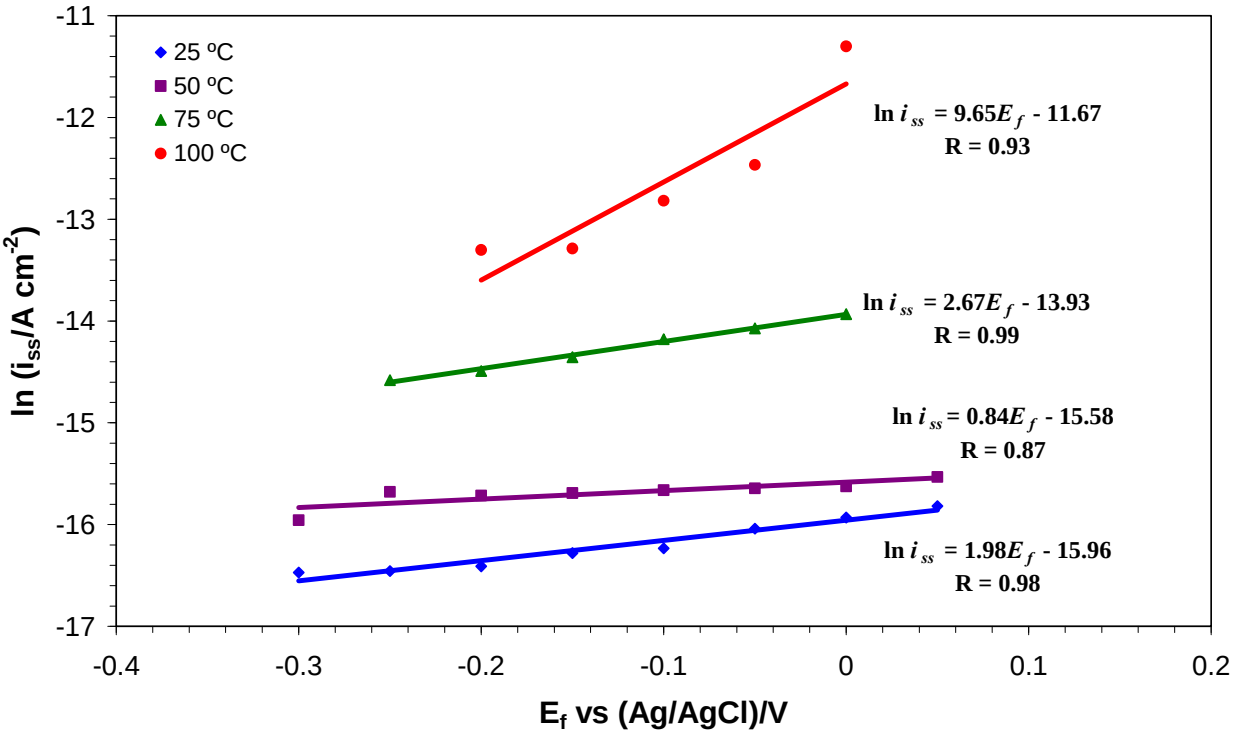

Figure 5

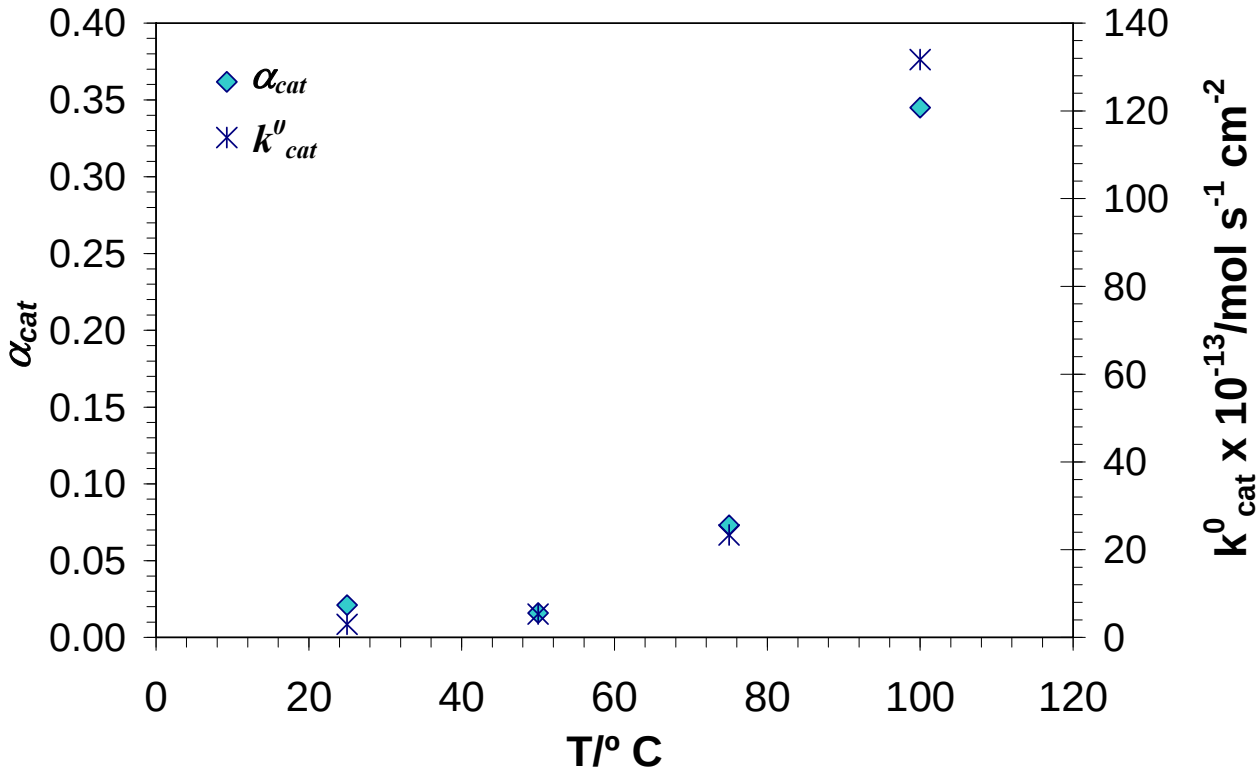

Figure 6

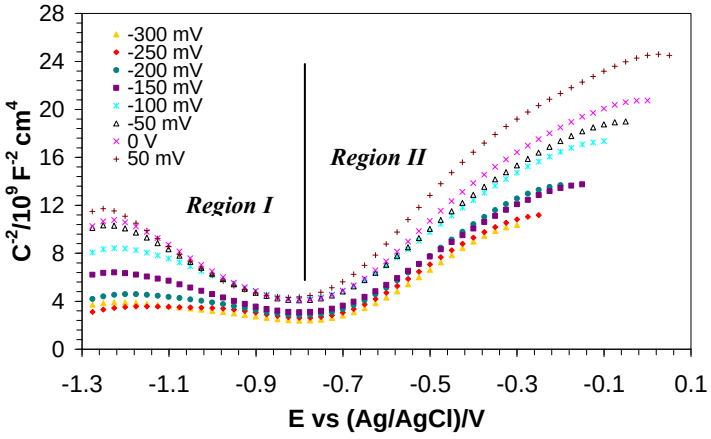

(a)

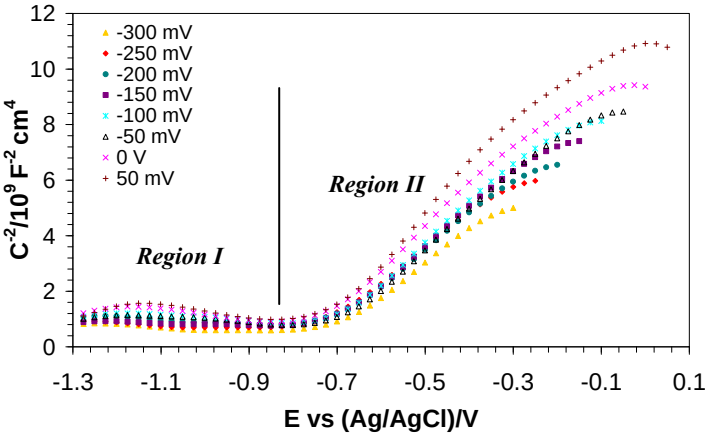

(b)

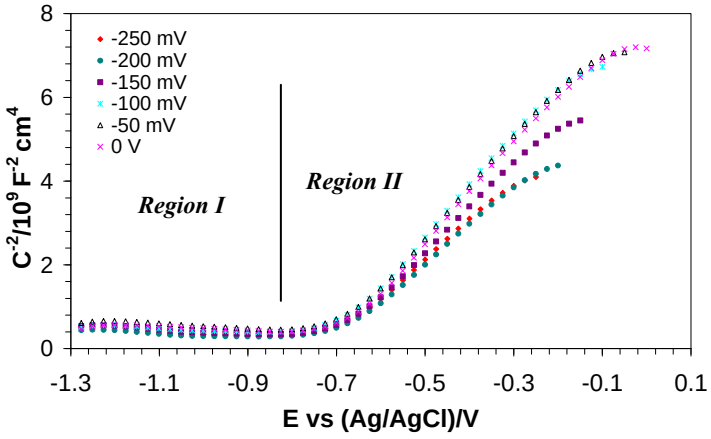

(c)

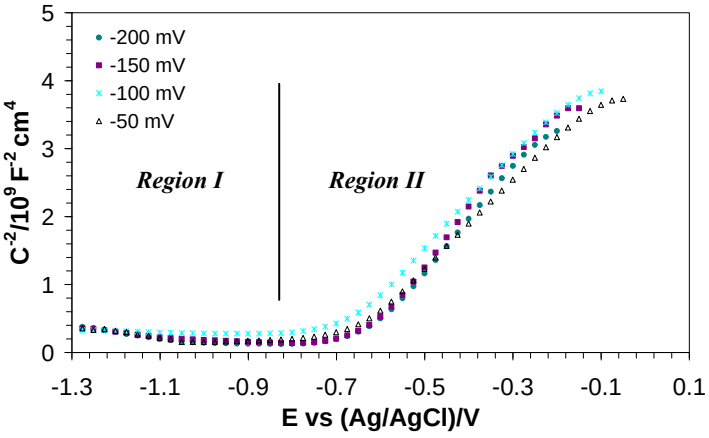

(d)

Figure 7

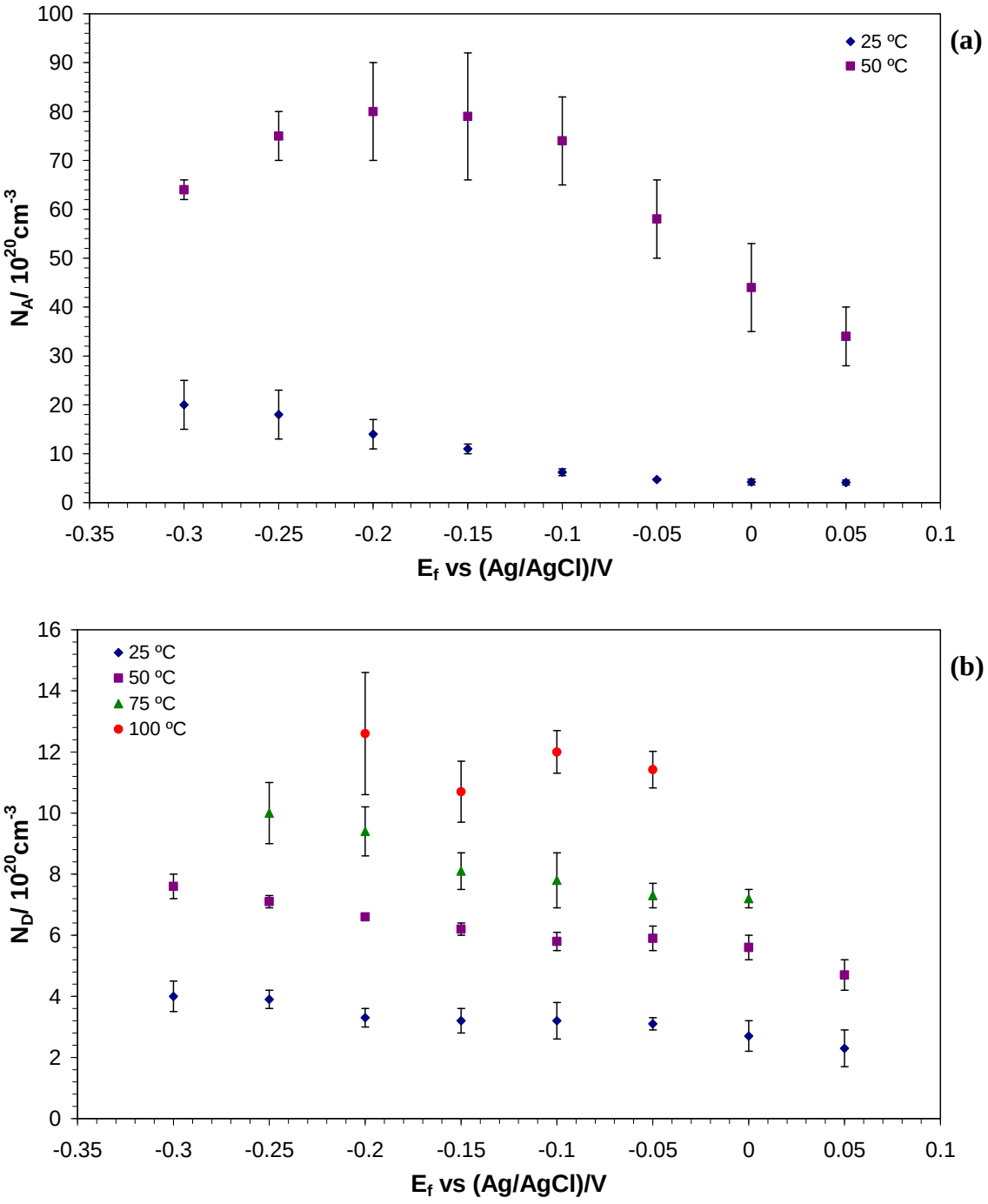
(a)
25 ºC
50 ºC
N_A/ 10^{20}cm^{-3}
E_f vs (Ag/AgCl)/V
(b)
25 ºC
50 ºC
75 ºC
100 ºC
N_D/ 10^{20}cm^{-3}
E_f vs (Ag/AgCl)/V

Figure 8

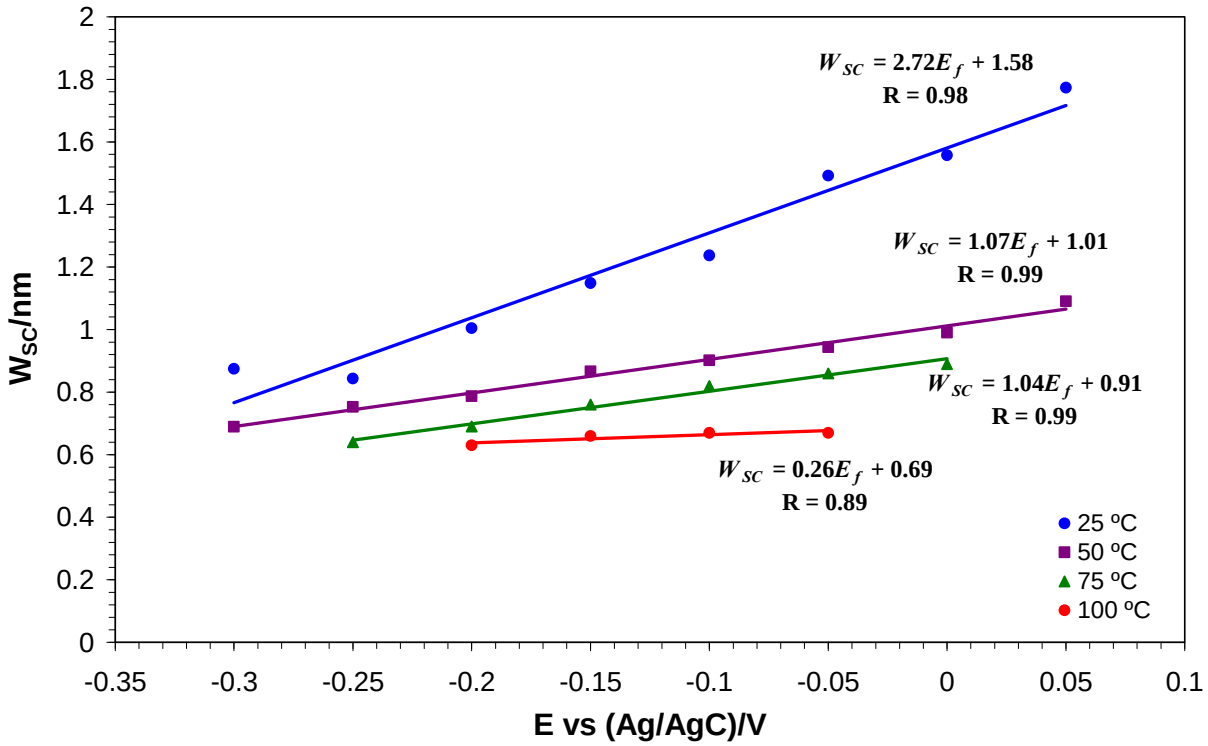

Table 1

C_{LiBr}/g l^{-1}	C_{LiBr}/mol l^{-1}	T/ºC	m_{LiBr}/(mol LiBr) (kg H_2O)$^{-1}$	$\gamma_{\pm}$	a_{LiBr}
100	**1.15**	25	1.20	0.81	0.98
		50	1.21	0.81	0.98
		75	1.10	0.78	0.86
400	**4.61**	25	5.69	3.53	20.12
		50	5.74	3.08	17.67
		75	5.79	2.64	15.28
700	**8.06**	25	10.18	18.95	192.88
		50	10.34	14.30	147.96
		75	10.50	10.43	109.45
		100	10.68	7.49	80.02
992	**11.42**	25	15.15	89.26	1352.56
		50	15.53	60.21	935.34
		75	15.84	38.31	606.72
		100	16.20	23.92	387.65

Table 2

	25 ºC		50 ºC		75 ºC		100 ºC	
***E* vs (Ag/AgCl)/V**	W_p / nm	W_n / nm	W_p / nm	W_n / nm	W_p / nm	W_n / nm	W_p / nm	W_n / nm
-0.30	0.14 ± 0.05	0.73 ± 0.03	0.05 ± 0.01	0.64 ± 0.02	-----	-----	-----	-----
-0.25	0.09 ± 0.03	0.75 ± 0.08	0.05 ± 0.01	0.70 ± 0.05	-----	0.64 ± 0.02	-----	-----
-0.20	0.12 ± 0.03	0.88 ± 0.05	0.06 ± 0.02	0.73 ± 0.01	-----	0.69 ± 0.02	-----	0.63 ± 0.04
-0.15	0.30 ± 0.06	0.85 ± 0.07	0.06 ± 0.01	0.81 ± 0.07	-----	0.76 ± 0.04	-----	0.66 ± 0.03
-0.10	0.31 ± 0.04	0.93 ± 0.07	0.06 ± 0.02	0.84 ± 0.05	-----	0.82 ± 0.05	-----	0.67 ± 0.06
-0.05	0.47 ± 0.02	1.02 ± 0.09	0.06 ± 0.02	0.88 ± 0.02	-----	0.86 ± 0.02	-----	0.67 ± 0.04
0	0.45 ± 0.01	1.11 ± 0.07	0.07 ± 0.03	0.92 ± 0.04	-----	0.89 ± 0.05	-----	-----
0.05	0.52 ± 0.04	1.25 ± 0.09	0.09 ± 0.03	1.00 ± 0.04	-----	-----	-----	-----